ORIGINAL ARTICLE

In vivo quantification of neuro-glial metabolism and glial glutamate concentration using ^{1}H-[^{13}C] MRS at 14.1T

Bernard Lanz,* Lijing Xin,* Philippe Millet† and Rolf Gruetter*,‡,§

Laboratory for Functional and Metabolic Imaging (LIFMET), Ecole Polytechnique Fédérale de Lausanne, Lausanne, Switzerland

†Unité de Neurophysiologie et Neuroimagerie, Hôpitaux Universitaires de Genève, Geneva, Switzerland

‡Department of Radiology, University of Lausanne, Lausanne, Switzerland

§Department of Radiology, University of Geneva, Geneva, Switzerland

Abstract

Astrocytes have recently become a major center of interest in neurochemistry with the discoveries on their major role in brain energy metabolism. An interesting way to probe this glial contribution is given by *in vivo* ^{13}C NMR spectroscopy coupled with the infusion labeled glial-specific substrate, such as acetate. In this study, we infused alpha-chloralose anesthetized rats with [2-^{13}C]acetate and followed the dynamics of the fractional enrichment (FE) in the positions C4 and C3 of glutamate and glutamine with high sensitivity, using ^{1}H-[^{13}C] magnetic resonance spectroscopy (MRS) at 14.1T. Applying a two-compartment mathematical model to the measured time courses yielded a glial tricarboxylic acid (TCA) cycle rate (V_g) of 0.27 ± 0.02 µmol/g/min and a glutamatergic neurotransmis-sion rate (V_{NT}) of 0.15 ± 0.01 µmol/g/min. Glial oxidative ATP metabolism thus accounts for 38% of total oxidative metabolism measured by NMR. Pyruvate carboxylase (V_{PC}) was 0.09 ± 0.01 µmol/g/min, corresponding to 37% of the glial glutamine synthesis rate. The glial and neuronal transmitoc-hondrial fluxes (V_x^g and V_x^n) were of the same order of magnitude as the respective TCA cycle fluxes. In addition, we estimated a glial glutamate pool size of 0.6 ± 0.1 µmol/g. The effect of spectral data quality on the fluxes estimates was analyzed by Monte Carlo simulations.

Keywords: ^{13}C MRS, acetate metabolism, glial TCA cycle, glutamate/glutamine cycle, metabolic modeling, neurotrans-mission.

J. Neurochem. (2014) **128**, 125–139.

The brain, which is one of the most energy demanding organs in mammals, is the center of a very complex neuronal network which accomplishes the major part of the treatment of sensory information and motor functions as well as a large amount of cognitive functions, including memory, solving problems and making decisions. All these cerebral functions are the result of an intense electrochemical interaction between two major cell types, neurons and glial cells. In traditional neuroscience of the 20th century, the standard picture of brain function was that the neurons accomplish the numerous cerebral tasks, while the glial cells are simply responsible to maintain the neuronal environment in good conditions to enable proper neurotransmission. However, several studies changed this conception and showed that glial cells are active elements of the neurotransmission process (Shank *et al.* 1993; Yudkoff *et al.* 1993). Glial cells are in particular involved in the glutamate-glutamine cycle, where they are responsible for the uptake of glutamate (the major excitatory neurotransmitter) from the synaptic cleft and its

ORIGINAL ARTICLE

conversion to the electrophysiologically inactive glutamine. The maintenance of the neurotransmission processes requires energy, delivered by glycolysis and the neuronal and glial tricarboxylic acid (TCA) cycle from glucose, which is the major energy substrate for the brain (Sokoloff 1977). However, glial cells are also fueled by alternative substrates, such as acetate (Badar-Goffer *et al.* 1990; Cerdan *et al.* 1990). More recent studies have shown evidences for the particular versatile function of astrocytes in brain energy metabolism; their capabilities to use a wide range of energy substrates (McKenna 2012) and to adapt their metabolism under pathological conditions (Gulanski *et al.* 2013; Jiang *et al.* 2013). *In vivo* ^{11}C-acetate infusion experiments also showed an increased washout rate of the produced ^{11}C-labeled metabolites under neuronal activation, pointing to an increase of astrocytic oxidative metabolism (Wyss *et al.* 2009), yet without demonstrating the quantitative relationship between the washout rate and glial $CMRO_2$. Recent developments have been therefore undertaken to enable the biochemical interpretation of ^{11}C-acetate uptake curves (Lanz *et al.* 2012). As a consequence, acetate might become in the near future a substrate of choice to probe modifications of glial energy metabolism in neurologic patients, insofar a detailed biochemical understanding of the observed metabolite labeling is achieved.

Two-compartment modeling combined with dynamic ^{13}C magnetic resonance spectroscopy (MRS) has proven to be a powerful tool to probe brain oxidative metabolism and neurotransmission, both in human and rodent studies (Gruetter *et al.* 2001; Henry *et al.* 2006). Most of these studies used ^{13}C labeled glucose as substrate to determine neuroglial metabolic fluxes (Gruetter *et al.* 2001; Choi *et al.* 2002; Henry *et al.* 2002; de Graaf *et al.* 2003a, 2004; Oz *et al.* 2004; Duarte *et al.* 2011). Since glucose is metabolized both in neurons and glial cells, the labeling of the glutamate and glutamine carbon positions is reflecting a mixture of the metabolic flow through the glial and neuronal TCA cycles. Depending on the number of measured turnover curves and on the experimental conditions, some of the determined metabolic fluxes can be subject to high uncertainties and might be unreliable as discussed by (Shestov *et al.* 2007; Duarte *et al.* 2011). This issue was especially raised for the glutamate-glutamine cycle flux.

Acetate is specifically taken up by the glia (Waniewski and Martin 1998) and thus is an ideal substrate to probe glial oxidative metabolism and to potentially increase the sensitivity of the measurement of the glutamate-glutamine cycle (Araque *et al.* 1999; de Graaf *et al.* 2003b; Henry *et al.* 2006). When infusing ^{13}C labeled acetate, glutamine becomes the labeling precursor of the large neuronal glutamate pool, whose turnover dynamics is therefore very sensitive to the glutamatergic neurotransmission rate.

When infusing [2-^{13}C]acetate, the first amino acid position to be labeled is the C4 of the small glial glutamate pool, which quickly labels the C4 of glial glutamine. The transfer of ^{13}C to glial glutamate C4 is the result of two processes, namely the activity of the glial TCA cycle (represented by $V_{tca}^g = V_g + V_{PC}$) and the tracer exchange between 2-oxoglutarate in the glial TCA cycle and the cytosolic glutamate (represented by V_x^g). If only the positions C4 of glutamate and glutamine are measured, metabolic modeling enables the determination of the composite flux V_{gt}^g [$V_{gt}^g = V_x^g \cdot V_{tca}^g / (V_x^g + V_{tca}^g)$], while assumptions on the exchange flux V_x^g have to be made to extract V_{tca}^g (Uffmann and Gruetter 2007; Lanz *et al.* 2012).

Additional information on the individual values of the glial TCA cycle rate and the glial exchange rate V_x^g requires the measurement and mathematical modeling of the C3 enrichment curves, similar to what was previously shown in one-compartment brain metabolic modeling (Henry *et al.* 2006; Uffmann and Gruetter 2007). The slope of the initial part of the neuronal glutamate C3 turnover curve is indicative of the V_x^n / V_{tca}^n ratio. In a similar way, the turnover of glial glutamate C3 and its direct product glutamine C3 carries information on the V_x^g / V_{tca}^g ratio. The simultaneous measurement of the time course of the C4 and C3 positions of glutamate and glutamine is therefore a necessary condition to determine both TCA cycle fluxes with minimal assumptions. With infusion of ^{13}C labeled acetate, the precision of the estimated glial metabolic fluxes is also expected to be higher than with ^{13}C glucose, where label incorporation into the glutamate-glutamine cycle is heavily weighted by the strong activity of the neuronal TCA cycle.

In all previous ^{13}C MRS studies using ^{13}C-acetate infusion in rats, the ^{13}C uptake curves of the labeling position C3 of glutamate and glutamine could not be determined directly *in vivo*, preventing the determination of the exchange rates V_x^g and V_x^n. In some studies, the metabolic fluxes were extracted from data acquired at metabolic steady-state (Patel *et al.* 2005), which allows only the determination of relative metabolic rates (ratios like V_{NT} / V_{tca}^n). Other studies measured the glutamate and glutamine C3 enrichments *ex vivo* in a separate group of animals, at limited time points (typically one or two) (Patel *et al.* 2010) or using coinfusion of ^{13}C labeled glucose and acetate (Deelchand *et al.* 2009a), which results in a higher NMR signal with a complex isotopomer pattern, to which an extended metabolic modeling approach needs to be developed (Shestov *et al.* 2012). Finally, sequential infusion of ^{13}C-labeled glucose and acetate in two different animal groups were undertaken with a common modeling (van Eijsden *et al.* 2010), where the steady-state enrichment following [2-^{13}C]acetate infusion was used as a constraint for the modeling of the [U-^{13}C]glucose dynamic data.

The difficulty of acquiring dynamic labeling data directly using ^{13}C-acetate infusion is linked to the predominant glial metabolism of acetate and the large inflow of unlabeled carbons through the dominating neuronal TCA cycle, which

results in a strong dilution of the labeling in glutamate and glutamine and thus to a reduction of the measured ^{13}C signal. Not surprisingly, most *in vivo* ^{13}C-acetate brain studies were thus performed with indirect detected ^{13}C NMR using the related increased sensitivity (Deelchand *et al.* 2009b; Patel *et al.* 2010). However, if indirect ^{13}C detection enables a significant gain in sensitivity by measuring the protons attached to the ^{13}C nuclei, its intrinsically low spectral resolution often makes it impossible to distinguish between certain labeling positions, like the C3 resonances of glutamate and glutamine.

The aim of this study was to take advantage of the increased spectral resolution obtained at 14.1T (see Fig. 2a) to measure *in vivo* and separately the turnover of the C4 and C3 positions of glutamate and glutamine to assess neuroglial metabolism, using an infusion of [2-^{13}C]acetate. A major objective was to determine the glial and neuronal transmitochondrial exchange rates V_x^g and V_x^n. A second aim was to use the high sensitivity of the turnover curves to determine for the first time the glial glutamate pool size in rat brain tissue. Finally, Monte Carlo simulations were used to assess the precision of the determined metabolic fluxes and further to investigate the evolution of this precision with changes in the experimental conditions (experiment duration, SNR, and temporal resolution).

Materials and methods

The metabolic modeling presented in this study is based on MRS data previously acquired with a newly developed full signal intensity ^{1}H-[^{13}C] NMR sequence (Xin *et al.* 2010). For completeness sake, the animal preparation and NMR acquisition protocols are briefly described below.

Animal preparation

All animal experiments were approved by the veterinary authorities of the Canton of Vaud and were performed in accordance with their guidelines. The experiments were performed by licensed investigators. Six healthy male Sprague–Dawley rats (263 ± 19 g, mean ± standard deviation, Charles River Laboratories, L'Arbresle, France) were fasted overnight (15–16 h), with free access to water before the studies. Animals were intubated and ventilated with 2% isoflurane during the surgery. Both femoral veins were catheterized for continuous infusion of α-chloralose (Fisher Scientific, Pittsburgh, PA, USA) and 99% enriched [2-^{13}C]sodium acetate (Sigma-Aldrich, St. Louis, MO, USA). One femoral artery was cannulated for blood sampling. After preparation, anesthesia was achieved by an 80 mg/kg initial bolus of α-chloralose, followed by continuous infusion at a rate of ~26.7 mg/kg/h. The animal was placed in a homemade holder and the head was stereotaxically fixed. Respiration rate and blood pressure were continuously monitored (SA Instruments Inc., Stony Brook, NY, USA). Body temperature was measured by a rectal thermosensor and maintained at 38.0 ± 0.5°C by circulating heated water. A variable bolus of 3M 99% enriched [2-^{13}C]sodium acetate (pH = 6) was given over two consecutive 5-min periods, with rates of 1.8 mmol/min/kg and 1.1 mmol/min/kg,

respectively, and then a continuous rate of 0.3 mmol/min/kg was applied. The infused volume of acetate solution was ~5 mL in total. Arterial blood (200 μL) was sampled approximately every 30 min for monitoring blood gases (pCO$_2$ = 39 ± 2 mm Hg, pO$_2$ > 100 mm Hg), pH (7.41 ± 0.03), and the analysis of plasma acetate concentration and isotopic enrichment, measured with high-resolution NMR spectroscopy (Xin *et al.* 2010). An aliquot of arterial blood was immediately centrifuged and stored in a nearby −80°C freezer for subsequent processing. The total amount of blood withdrawn was below 10% of the total blood volume of the rat.

In vivo ^{13}C MRS acquisition

All experiments were carried out on an animal magnetic resonance imaging system (Varian, Palo Alto, CA, USA) interfaced to a 14.1 T, 26 cm, horizontal-bore magnet (Magnex Scientific, Oxford, UK) with actively shielded gradients (12 cm inner diameter, 400 mT/m in 120 μs). A homemade 13 mm diameter geometrically decoupled quadrature ^{1}H surface coil with a 10 mm diameter single-loop linear ^{13}C coil was used as both transmitter and receiver. Fast spin-echo images (effective TE = 45 ms, echo train length = 8, pulse repetition time = 2.5 s, number of transitions = 2, slice thickness = 1 mm, field of view = 30 × 30 mm^2, matrix = 256 × 256) were acquired for positioning of the volume of interest. Localized ^{1}H{^{13}C} spectra were acquired from a volume of 144 μL (8 × 3 × 6 mm^3) centered in cerebral cortex of the rat brain. To optimize the magnetic field homogeneity in the volume of interest, an echo-planar imaging version of FASTMAP (Gruetter and Tkac 2000) was used to adjust all first- and second-order shims, which achieved a full width at half maximum of the water signal of 20–22 Hz *in vivo*. During 150 min of 99% enriched [2-^{13}C]sodium acetate infusion, ^{13}C enrichment (GluC4, GlnC4, GluC3, GlnC3, AceC2) and total concentration of glutamate, glutamine, and acetate were acquired using the SPECIAL-BISEP ^{1}H{^{13}C} NMR sequence. For a detailed description of this pulse sequence and the related spectral quantification, we refer the reader to our previously published work (Xin *et al.* 2010).

Metabolic modeling

Metabolic modeling was developed based on the compartmentalized neurotransmitter approach (Gruetter *et al.* 2001; Sibson *et al.* 2001). Brain tissue is mainly composed of glial and neuronal cells. It is now well established that glial cells are actively involved in glutamate neurotransmission, for example, through the uptake of the major excitatory neurotransmitter glutamate from the synaptic cleft (Arriza *et al.* 1994; Rothstein *et al.* 1996; Hertz 2011). The model therefore consists of two main metabolic compartments corresponding to each type of cell. Each compartment consists of the respective TCA cycle and both compartments are linked by the glutamate-glutamine cycle, responsible for the neurotransmission.

Acetate has the particularity to be metabolized almost purely in astrocytes (glial compartment) (Badar-Goffer *et al.* 1990; Hassel *et al.* 1995; Waniewski and Martin 1998; Lebon *et al.* 2002). As a consequence, the inflow of new ^{13}C label from the substrate is occurring through the glial TCA cycle. The neuronal TCA cycle provides unlabeled carbons originating from neuronal pyruvate metabolism to the glutamate-glutamine cycle. However, ^{13}C flow from the carbon position 4 of glutamate to the position 3 occurs both in the glial and neuronal compartment (see Appendix and Fig. 1b).
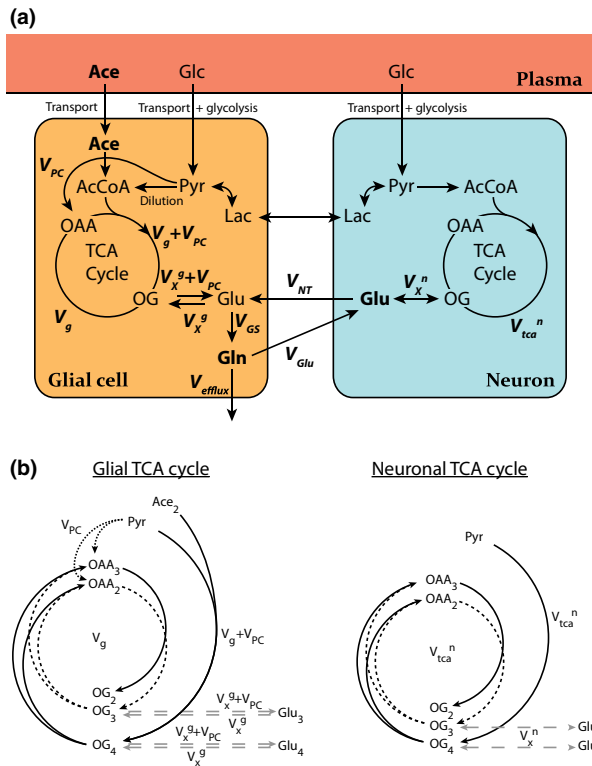
(a)

(b)

Fig. 1 (a) Schematic view of the two-compartment model used to describe the dynamic ^{13}C MRS data acquired in the brain after [2-^{13}C] acetate infusion. Acetate is transported across the blood brain barrier and is metabolized to acetyl-CoA, which enters the glial tricarboxylic acid (TCA) cycle at the level of citrate. V_g is the TCA cycle rate in the glia, V_{tca}^n the TCA cycle rate in the neuronal compartment. The transmitochondrial exchange rates V_x^g and V_x^n model the exchange between amino acids and 2-oxoglutarate, in the glial and neuronal compartment, respectively. In the glial compartment, V_{PC} represents the pyruvate carboxylase, responsible for anaplerosis. V_{GS} is the glutamine synthesis flux and V_{Glu} summarizes the transport of glutamine to the neurons and its conversion to glutamate. V_{NT} is the apparent glutamatergic neurotransmission rate. Finally, efflux of labeling from the metabolic system occurs through the rate of glial glutamine loss V_{efflux}. (b) Detailed view of the label scrambling from [2-^{13}C]acetate between the C4 and C3 positions of glutamate (Glu) in the glial and neuronal TCA cycle. ^{13}C enters in the glial compartment, is incorporated in the glial TCA cycle and labels 2-oxoglutarate (OG) at the position C4 in the first turn of the TCA cycle. Through transmitochondrial transport, OG is in exchange with the cytosolic Glu which gets labeled at the position C4. After the second turn of the glial TCA cycle, OG C3 is labeled from OG C4. This labeling pathway is diluted by the action of pyruvate carboxylase, bringing unlabeled carbons from pyruvate to the position C3 of oxaloacetate. Through transmitochondrial, glial Glu C3 is labeled from OG C3. The neuronal TCA cycle acts similarly, with the difference that no ^{13}C from acetate enters the first turn of the TCA cycle and that pyruvate carboxylase is absent from the neuronal compartment.

The resulting model is presented in Fig. 1a. To illustrate how label is transferred within a molecule in the TCA cycle, we added the detailed scheme in Fig. 1b. ^{13}C from [2-^{13}C]acetate enters the glial

TCA cycle at the position 4 of citrate. In the first turn of the TCA cycle, ^{13}C-reaches the position 4 of 2-oxoglutarate with a total net flux $K_{dil}(V_g+V_{PC})$ (Appendix, eqn (10)), where K_{dil} represents the affinity of glial metabolism to acetate. K_{dil} was fixed to 0.76, as previously found in ^{13}C *in vivo* brain studies using [1,6-^{13}C$_2$] glucose infusion (Duarte *et al.* 2011). Similarly, in a previous ^{13}C-acetate infusion study (Deelchand *et al.* 2009b), it was estimated that about 80% of acetyl-CoA entering the glial TCA cycle is synthesized from [2-^{13}C]acetate, while the remaining 20% is synthesized from unlabeled glucose, in similar physiological conditions. 2-oxoglutarate exchanges label with cytosolic glutamate. This transmitochondrial label exchange, denoted by V_x^g, transfers label from the carbon position 4 of 2-oxoglutarate to the position 4 of glutamate. As a result of the symmetry of the succinate molecule, the second turn of the TCA cycle brings half of the labeled carbons of the position 4 of 2-oxoglutarate to the position 3 of 2-oxoglutarate and half to the position 2 of 2-oxoglutarate, further eliminated as ^{13}CO$_2$. Through the transmitochondrial flux V_x^g, [3-^{13}C]glutamate is formed from [3-^{13}C]2-oxoglutarate. Pyruvate carboxylase brings unlabeled ^{12}C from pyruvate to oxaloacetate, which further dilutes the position C3 of glial glutamate. Pyruvate carboxylase is also responsible to maintain the balance of mass in the glial TCA cycle and compensates the label efflux from glutamine or contributes to a possible accumulation in the amino acids concentrations.

When glutamate and glutamine total concentrations are constant (metabolic steady-state), the mass balance is given by the following:

$V_{GS} = V_{NT} + V_{PC}$	(1)	Steady-state of glial glutamate
$V_{Glu} = V_{NT}$	(2)	Steady-state of neuronal glutamate
$V_{efflux} = V_{GS} - V_{Glu} = V_{PC}$	(3)	Steady-state of glutamine

On the neuronal side, label entering the TCA cycle in the first turn from acetate is neglected, consistent with the glial-specific uptake of acetate. Nevertheless, once neuronal glutamate is sufficiently labeled by the action of the glutamate-glutamine cycle, the exchange between glutamate and 2-oxoglutarate through V_x^n allows a labeling of the glutamate at position 3 from the glutamate at position 4 in the second turn of the TCA cycle, similar to what happens in the glial TCA cycle [Appendix, eqn (23)].

A system of linear differential equations was derived for this two-compartment model, assuming constant metabolic fluxes. As previously shown (Uffmann and Gruetter 2007), the temporal change in labeling of the TCA intermediates present in low concentration can be eliminated from the mathematical model without modifying the labeling dynamics of glutamate, resulting in a 6-pools model (Glu$_4^g$, Glu$_3^g$, Gln$_4$, Gln$_3$, Glu$_4^n$, Glu$_3^n$). The detailed derivation of the labeling equations is provided in the appendix.

The NMR-measured brain AceC2 enrichment was fitted by an exponential function multiplied with a linear function, to take into account the slow increase in AceC2 fractional enrichment (FE) in the later part of the experiment (see Fig. 2b). The fitted AceC2 curve was used as direct input function for the metabolic system. The time
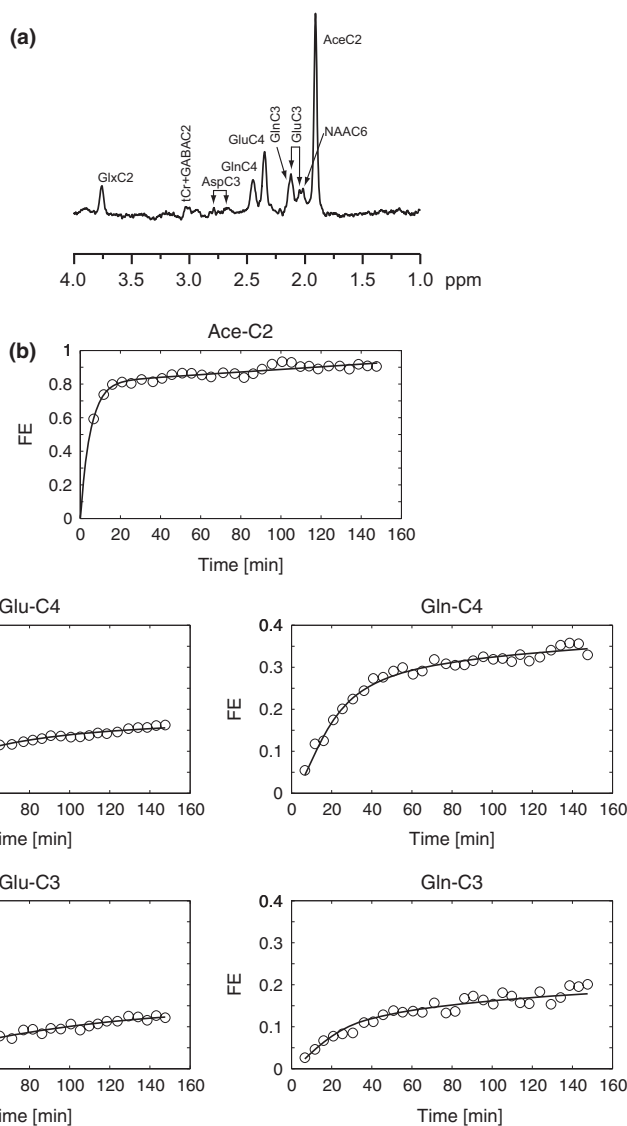
Fig. 2 (a) Example of *in vivo* edited ^{1}H-[^{13}C] MRS spectrum acquired at 14.1T in a 144 μL voxel centered in cerebral cortex of a rat. The data were averaged over 45 min, about 105 min after the beginning of the [2–^{13}C]acetate infusion. This spectrum illustrates the higher spectral resolution achieved at high magnetic field, enabling the separate quantification of AceC2, GluC4, GlnC4, GluC3, and GlnC3. See (Xin *et al.* 2010) for details on this MRS acquisition method. (b) Fit of the model presented in figure 1 to the time courses of fractional enrichment (FE) of glutamate and glutamine positions C4 and C3, averaged over six rats, using the measured brain AceC2 as input function. Glutamate enrichment curves represent the sum of the glial and neuronal glutamate pools, while the glutamine enrichment curves are modeled as purely glial (see discussion). AceC2 was smoothed by fitting it with a function of the type $y(t) = (a \cdot t + b)(1 - e^{-k \cdot t})$, to take into account the slow increase in FE measured in the second part of the curve.

courses of total glutamate and glutamine were fitted with a linear function and used in the modeling as constraints in the mass balance equations. The two-compartment model was therefore adapted to include an increased mass flow through pyruvate carboxylase in the glial compartment (see Appendix). In practice, using the measured accumulation rate in glutamate ($\frac{dGlu}{dt}$) and in glutamine ($\frac{dGln}{dt}$), the following mass balance equations were set as new constraints in the model:

$$V_{GS} - V_{efflux} - V_{Glu} = \frac{dGln}{dt} \tag{4}$$
$$\text{with } V_{GS} = V_{NT} + V_{PC}$$

$$V_{Glu} - V_{NT} = \frac{dGlu}{dt} \tag{5}$$

where it is assumed that accumulation of glutamate and glutamine takes place in the respective larger compartment (neuronal compartment for glutamate and glial compartment for glutamine) (Storm-Mathisen *et al.* 1992).

With these constraints, the metabolic system is characterized by 6 independent fluxes (V_g, V_x^g, V_{NT}, V_{tca}^n, V_x^n, V_{PC}).

The model was developed using Matlab (MathWorks, Natick, MA, USA). The model was fitted to the measured turnover curves, using a standard built-in ordinary differential equation solver and a modified Levenberg-Marquardt non-linear regression method. The fitting procedure was weighted with the square root of the inverse of the variance of the experimental noise, in order to take into account the different precisions in the measurement of the 4 turnover curves.

Glial glutamate fraction

In two-compartment modeling of brain metabolism, the glial and neuronal glutamate pools are linked to their respective TCA cycle and are therefore labeled differently. However, the proportion of the measured total glutamate which is located in the glial compartment cannot be assessed directly from ^{1}H MRS. Usually, this concentration is assumed as a fraction of the total measured glutamate (between 1.5% (Patel *et al.* 2010) and 14% (Gruetter *et al.* 2001)),

or fixed to a certain concentration (between 0.2 and 1.25 µmol/g (Sibson *et al.* 2001)).

Since ^{13}C from acetate enters through the glial TCA cycle, the turnover curves are expected to be especially sensitive to glial parameters. Furthermore, the glial glutamate pool is the labeling precursor of glutamine. The early glutamate FE time points are thus expected to reflect mainly the glial component of glutamate, before the large neuronal contribution starts to dominate.

The fit of the experimental data was therefore repeated for a range of glial glutamate concentrations varying between 0.08 and 1.5 µmol/g. The weighted residual sum of squares of the fit was then calculated for each of the assumed glial concentrations. The lowest fit residual was selected as an estimate of the glial glutamate concentration in the considered brain region. For the other parts of our study, the glial glutamate pool size was then fixed to this optimized value.

Influence of the experimental conditions on the flux precision

To evaluate the effect of the experiment duration, the temporal resolution and the noise level of the turnover curves on the precision of the fluxes, an extended Monte Carlo analysis was undertaken on synthetic turnover curves. Artificial GluC4, GluC3, GlnC4, and GlnC3 FE time courses were generated with the differential system characterizing the model, using the flux values and metabolite concentrations obtained on the experimental data ($V_g = 0.27$, $V_x^g = 0.17$, $V_{NT} = 0.15$, $V_{tca}^n = 0.37$, $V_x^n = 0.46$, $V_{PC} = 0.087$ µmol/g/min, [Gln] = 3.4 µmol/g and [Glu] = 11.5 µmol/g, from which 0.6 µmol/g was assumed to be in the glial compartment). A characteristic Gaussian noise of standard deviation $\sigma = 0.05$ µmol/g and $\sigma = 0.10$ µmol/g was added to the C4 and C3 turnover curves, respectively, as measured from the experimental data (Xin *et al.* 2010). A typical experiment duration of 150 min and a temporal resolution of 5 min were assumed as standard conditions.

Starting from these initial conditions, different experimental conditions were simulated by generating the GluC4, GluC3, GlnC4, and GlnC3 turnover curves varying either the length of the experiment (from 60 to 450 min), the time resolution (from 1.5 to 30 min) or by varying the noise level (from 0.2 to 5 times the original noise).

These sets of turnover curves were then fitted with the neuroglial metabolic model to obtain the best fit values for V_g, V_x^g, V_{NT}, V_{tca}^n, V_x^n, and V_{PC}, using the same minimization procedure as for the experimental data.

Statistical analysis

The standard deviation of the fitted flux values reported in this study were obtained from Monte Carlo simulations, based on fits of at least 100 artificial data (Mason and Rothman 2004). These data are synthetic GluC4, GluC3, GlnC4, and GlnC3 enrichment time courses, generated with the flux values obtained with the best fit, to which a gaussian noise of same variance σ^2 than the corresponding experimental turnover curves was added. The initial values of the fluxes were taken randomly between 0 and 1 µmol/g/min. The 95% confidence interval of the optimized glial glutamate concentration was calculated directly from the covariance matrix of the adjusted parameters obtained from the non-linear regression.

Results

To determine the precursor isotopic enrichment, plasma samples were measured with high-resolution NMR spectroscopy. The isotopic enrichment of AceC2 in blood reached 95% within 5 min after starting the infusion of [2-^{13}C]sodium acetate and was stable at around 90% during the whole experiment. The concentration of plasma acetate during the experiment was 9 ± 3 mM.

From the analysis of the unedited ^1H spectra and ^{13}C-edited ^1H spectra (64 averages), total concentration ($^{12}C + ^{13}C$) and the concentration of ^{13}C-labeled acetate and metabolites were obtained. The average concentrations obtained on the six animals were [Gln] = 3.4 µmol/g and [Glu] = 11.5 µmol/g.

The FE of brain acetate C2, used as input function, was reaching a first step at 80% after 15 min. After this first quick increase in FE, the enrichment of acetate C2 was linearly increasing to about 90% after 150 min.

During the infusion of sodium acetate, glutamate, and glutamine total concentrations were increasing with a rate of 0.018 and 0.004 µmol/g/min, respectively. The two-compartment model was therefore adapted to include an increased mass flow through pyruvate carboxylase in the glial compartment.

To determine the metabolic fluxes from the ^{13}C time courses, the two-compartment model presented in Fig. 1 was fitted to the FE turnover curves of the C4 and C3 positions of glutamate and glutamine (Fig. 2b) by adjusting the metabolic fluxes. The values of the determined metabolic fluxes are summarized in Table 1. Using brain acetate FE as input function, the model was able to accurately describe the measured turnover curves ($R^2 > 0.99$). The glutamine labeling positions were the first to be labeled, consistent with the dominant glial metabolism of acetate, since most glutamate is located in the neuronal compartment (Storm-Mathisen *et al.* 1992), whereas astrocytes contain most of the glutamine. The C4 positions were more enriched both in glutamate and in glutamine. The maximal FE reached by GlnC4 at the end of the experiment was 34%, while GluC3, the strongest diluted labeling position measured in this study, reached only 12%. Glutamine had a larger difference between the enrichments of C4 and C3 than glutamate, indicating that the glial-specific pyruvate carboxylase, diluting specifically the position C3, had a substantial activity compared with the glutamatergic neurotransmission rate.

An important factor in determining the metabolic fluxes is the glial glutamate concentration. To estimate its concentration, we varied the pool size of glial glutamate from 0.08 to 1.5 µmol/g and analyzed its effect on the weighted residual sum of squares of the fit (Fig. 3). It presents an optimum for a glial glutamate concentration of 0.6 ± 0.1 µmol/g. A 95% confidence interval was extracted from the fit statistics and places [Glu^g] in the range between 0.36 and 0.82 µmol/g.

Table 1 Determined metabolic fluxes (μmol/g/min) with reference to the model shown in figure 1. The errors were determined by Monte Carlo simulation, based on 500 artificial data sets, using experimentally determined noise levels for the synthetic glutamate and glutamine enrichment curves

Adjusted metabolic fluxes (in μmol/g/min)					
V_{g}	V_{x}^{g}	V_{PC}	V_{NT}	V_{tca}^{n}	V_{x}^{n}
0.27 ± 0.02	0.17 ± 0.02	0.087 ± 0.012	0.15 ± 0.01	0.37 ± 0.06	0.46 ± 0.05

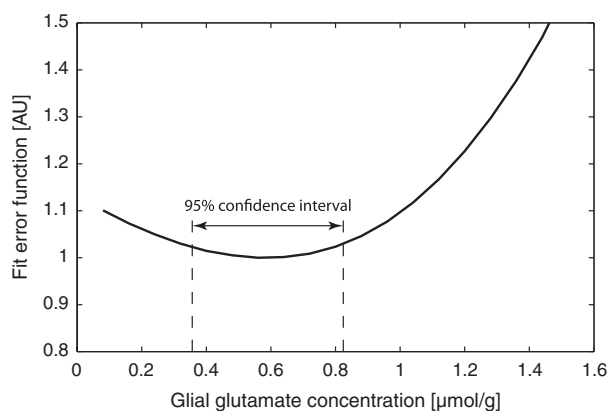| Derived metabolic fluxes (in μmol/g/min)			
V_{GS}	V_{tca}^{g}	V_{efflux}	V_{Glu}
0.24 ± 0.02	0.36 ± 0.03	0.065 ± 0.018	0.17 ± 0.01

Fig. 3 Evolution of the residual sum of squares with the assumed glial glutamate concentration. The fit error function was scaled with respect to the best fit residual sum of squares, which was found for a glial glutamate concentration of 0.6 μmol/g. Mathematically, this curve represents an orthogonal projection of the residual sum of squares function from the parameter space on the one-dimensional subspace of the glial glutamate concentration. A 95% confidence interval was estimated from the covariance matrix of the regression when adding glial glutamate concentration as a free parameter.

To determine how the precision of the metabolic fluxes depends on experimental conditions, we simulated the effect of experiment duration on the standard deviation of V_{g}, V_{x}^{g}, V_{NT}, V_{tca}^{n}, V_{x}^{n}, and V_{PC} when varying the measurement duration, from 60 to 450 min, and keeping a temporal resolution of 5 min and an experimentally determined standard noise level of 0.05 μmol/g and 0.1 μmol/g for the C4 and C3 turnover curves, respectively (Fig. 4a). When data were measured during less than 150 min, the neuronal flux across the mitochondrial membrane, V_{x}^{n}, was not reliably determined anymore. The precision of V_{tca}^{n} was reduced, evident from an increase of its relative error to 60% for 80 min of acquisition. Above the 150 min threshold, all the fitted fluxes presented a coefficient of variation below 25%. The glial TCA cycle flux V_{g} and the neurotransmission flux V_{NT} were throughout well determined (coefficient of variation of about 10%), even when a shorter experiment duration of less than 100 min was used.

When evaluating the influence of temporal resolution at a fixed experiment duration of 150 min and a noise level of 0.05 μmol/g and 0.1 μmol/g for the C4 and C3 turnover curves, respectively, we noted that the estimated value for the neuronal transmitochondrial flux V_{x}^{n} diverged for a temporal resolution lower than one measurement every 15 min (Fig. 4b). For the other metabolic fluxes, the reduction in temporal resolution resulted in a progressive deterioration of their precision with a maximal coefficient of variation of 55% for the glial transmitochondrial flux V_{x}^{g} at a temporal resolution of 30 min.

The effect of the noise level of the turnover curves was analyzed by multiplying the experimentally determined noise level (0.05 μmol/g for the C4 positions and 0.1 μmol/g for the C3 positions) by a noise factor N, varying between 0.2 and 5 (Fig. 4c). The transmitochondrial fluxes V_{x}^{g} and V_{x}^{n} were the most sensitive to the noise level. With more than a twofold increase in the noise level, the relative standard deviation of V_{x}^{g} and V_{x}^{n} became higher than 100%, which made their determination unreliable (Fig. 4c). V_{x}^{n} diverged already for a noise factor of 1.5 (0.075 μmol/g for the C4 positions and 0.15 μmol/g for the C3 positions). The glial and neuronal TCA cycle fluxes and the neurotransmission flux as well as the pyruvate carboxylase flux were progressively losing precision with the increase of the experimental noise, without presenting a critical point above which their uncertainties would suddenly increase. As observed for the experiment duration and the temporal resolution (see above), the glial TCA flux V_{g} and the neurotransmission flux V_{NT} were the most reliable fluxes determined with two-compartment modeling when infusing [2–^{13}C]acetate, with errors below 70% and 40%, respectively, for a noise factor of 5 (0.25 μmol/g for the C4 positions and 0.5 μmol/g for the C3 positions).

Discussion

In this study, we extended the sensitivity of detection and temporal resolution of the ^{13}C turnover curves of glutamate and glutamine under infusion of [2-^{13}C]acetate using a recently developed ^{1}H-[^{13}C] MRS localized detection
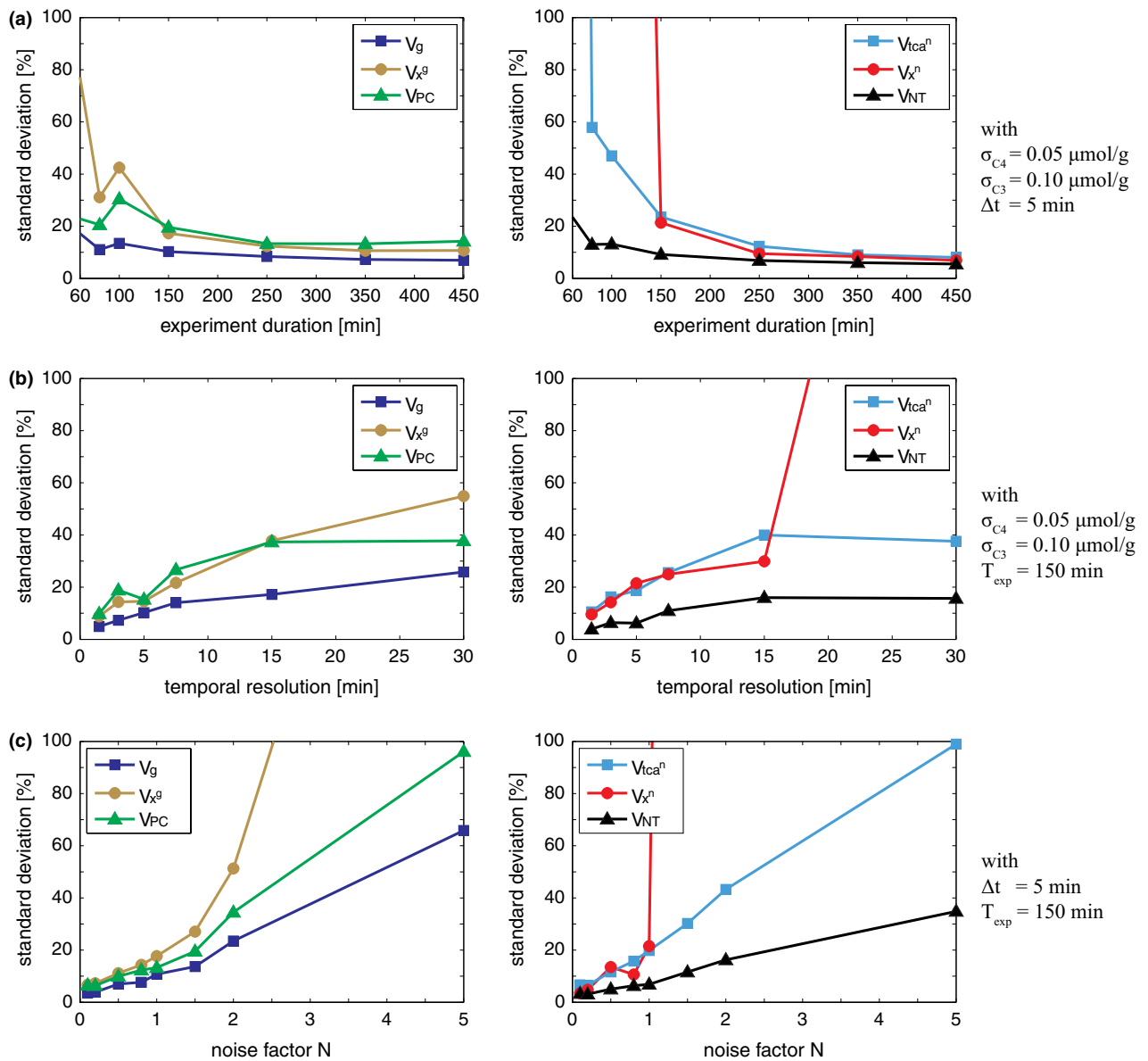
Fig. 4 Analysis of the precision in the determination of the glial (V_g, V_x^g, and V_{PC}) and neuronal (V_{tca}^n, V_x^n, and V_{NT}) metabolic fluxes as a function of the noise level, duration, and temporal resolution of the acquired labeling data. (a) Variation of the relative standard deviation of the 6 fitted metabolic fluxes with the experiment duration. This simulation was based on the fit of the 4 turnover curves (GluC4, GlnC4, GluC3, GlnC3), with a temporal resolution Δt of 5 min and a typical noise level of $\sigma_{C4} = 0.05$ μmol/g for the C4 positions and $\sigma_{C3} = 0.1$ μmol/g for the C3 positions of glutamate and glutamine. (b) Variation of the relative standard deviation of the 6 fitted metabolic fluxes with the temporal resolution. This simulation was based on the fit

of the 4 turnover curves (GluC4, GlnC4, GluC3, GlnC3), with an experimental duration T_{exp} of 150 min and a typical noise level of $\sigma_{C4} = 0.05$ μmol/g for the C4 positions and $\sigma_{C3} = 0.1$ μmol/g for the C3 positions of glutamate and glutamine. (c) Variation of the relative standard deviation of the 6 fitted metabolic fluxes with the noise level. This simulation was based on the fit of the 4 turnover curves (GluC4, GlnC4, GluC3, GlnC3), with an experimental duration T_{exp} of 150 min and a temporal resolution Δt of 5 min. The noise level (in μmol/g) is equal to the noise factor multiplied with a standard noise of $\sigma_{C4} = 0.05$ μmol/g for the C4 positions and $\sigma_{C3} = 0.1$ μmol/g for the C3 positions of glutamate and glutamine.

method at high magnetic field (14.1T). This detection method takes advantage of the higher spin polarization and spectral resolution obtained at 14.1T as well as the stronger gyromagnetic ratio of ^{1}H, as compared to ^{13}C. This technique

enabled the measurement of the ^{13}C turnover curves of glutamate and glutamine at position C4 and C3 as well as of acetate at position C2 with a temporal resolution of 4.5 min in a 144 μL voxel. The position C3 of glutamate and

glutamine could be measured separately and used in the metabolic modeling for the first time in an *in vivo* ^{13}C-acetate infusion experiment. From the two-compartment modeling of these uptake curves, a precise determination of the glial and neuronal TCA cycle fluxes, glial pyruvate carboxylase, as well as the apparent neurotransmission flux characterizing the neuroglial glutamate-glutamine exchange was possible. Moreover, based on the C3 enrichment curves, we could extend the metabolic modeling to measure separately the glial and neuronal transmitochondrial fluxes. Monte Carlo analysis demonstrated that the 6 adjusted metabolic fluxes are determined with high precision, with a maximal error of 16% for the neuronal TCA cycle flux (V_{tca}^n). In addition, we estimated a glial glutamate concentration of 0.6 μmol/g by minimization of the weighted residual sum of squares when varying the neuroglial distribution of the total measured glutamate.

Metabolic fluxes

The measurement of the C3 positions of glutamate and glutamine is particularly challenging in ^{13}C-acetate infusion experiments, since the large dilution of glutamate through the neuronal TCA cycle reduces considerably the FE of the turnover curves, compared to glucose infusion experiments. In the case of the C3 positions, a maximum FE of 20% was reached for GlnC3 at the end of the acquisition. This overall lower ^{13}C signal is a strong argument toward the use of the more sensitive indirect ^{13}C detection (de Graaf *et al.* 2003b). However, the lower spectral resolution of this method makes the separation of glutamate and glutamine C3 peaks difficult. Nevertheless, the higher magnetic fields NMR scanners as well as the improved shimming methodologies available today enable a reliable separation of these peaks (Xin *et al.* 2010), with a temporal resolution of about 4.5 min.

Glial V_g was 0.27 ± 0.02 μmol/g/min, which corresponds to more than half of the neuronal TCA cycle rate, supporting the significant role of glial resting oxidative metabolism (Danbolt 2001; Dienel 2011; Hertz 2011).

One goal of this study was to assess the transmitochondrial rate V_x, representing the exchange between cytosolic glutamate and 2-oxoglutarate in the TCA cycle, located in the mitochondrial matrix. This exchange is principally mediated by the malate-aspartate shuttle (Gruetter *et al.* 2001). V_x is in fact a composite representation of glutamate dehydrogenase, aspartate transaminase and transport across the membrane of the mitochondria. In previous studies, V_x was frequently assumed to be much larger than the TCA cycle rate V_{tca} (Hyder *et al.* 1996; Sibson *et al.* 1998; de Graaf *et al.* 2003a), as suggested by early results (Mason *et al.* 1992, 1995). This assumption leads to the fact that the labeling patterns of 2-oxoglutarate and glutamate follow each other without time lag, in both glial and neuronal compartments, which allows for simplification in the metabolic model but

may lead to underestimation of the TCA cycle fluxes (Uffmann and Gruetter 2007).

The determination of the transmitochondrial fluxes requires the measurement of the C3 turnover curves of glutamate and glutamine, which are especially sensitive to the transmitochondrial fluxes in the early part of the experiment (Henry *et al.* 2006). The measurement of the C4 positions only allows the assessment of the composite flux V_{gt} ($V_{gt} = \frac{V_x * V_{tca}}{V_x + V_{tca}}$)(Uffmann and Gruetter 2007), while assumptions have to be made on the value of the respective V_x. Several studies showed that the transmitochondrial flux is in the same order of magnitude than V_{tca} (Gruetter *et al.* 2001; Choi *et al.* 2002; Henry *et al.* 2002; Oz *et al.* 2004; Duarte *et al.* 2011). However, V_x was typically measured with a relatively poor precision, on the order of 30% or more. In this study, we could determine both glial and neuronal transmitochondrial fluxes V_x^g and V_x^n with a precision of < 12%. Both fluxes were on the same order of magnitude as the corresponding TCA cycle fluxes. This result is in very good agreement with previous *in vivo* ^{13}C glucose infusion study (Duarte *et al.* 2011) and is supported by recent ^{13}C glucose labeling studies in cultured astrocytes (Amaral *et al.* 2011) and *in vivo* ^{13}C-acetate MRS studies using dynamic polarization techniques (Mishkovsky *et al.* 2012). The use of the glial-specific ^{13}C-acetate substrate enabled the determination of V_x^g with an increased precision, compared to labeled glucose infusion studies.

In the glial compartment, the measured transmitochondrial flux V_x^g is significantly smaller than the TCA cycle flux V_{TCA}^g ($V_{TCA}^g = V_g + V_{PC}$ is the pyruvate dehydrogenase flux in the glial compartment), coherent with previous ^{13}C glucose labeling studies (Duarte *et al.* 2011). The glial malate-aspartate shuttle represented by V_x^g participates to the cytosolic NADH/NAD$^+$ balance required for the glycolysis in the glial compartment (Hertz *et al.* 2007), which produces pyruvate, a TCA cycle substrate. This observation supports the fact that the glial TCA cycle is fueled in a significant proportion by substrates which do not require reducing equivalent transport, such as acetate and fatty acids (Hertz *et al.* 2007).

Interestingly, although acetate is not a substrate of the pyruvate carboxylation pathway, it was possible to determine a pyruvate carboxylase flux V_{PC} = 0.087 ± 0.012 μmol/g/min. This was possible since pyruvate carboxylase dilutes specifically the position C3 of glial glutamate, while the position C4 remains unaffected (Fig. 1b). At steady-state, the FE of glutamine reaches the level of its direct precursor, glial glutamate. The effect of pyruvate carboxylase can be qualitatively observed by the C4 to C3 enrichment ratio being higher in glutamine than in glutamate at the end of the experiment. Although part of this difference could be explained by a higher V_x/V_{tca} ratio in the glial compartment than in the neuronal one, the metabolic model was unable to fully describe the dynamics of the 4 uptake curves without

the inclusion of the pyruvate carboxylase flux (data not shown). V_{PC} accounts for 37% of the rate of glutamine synthesis, a higher fraction than what has been recently reported in the human brain (Mason *et al.* 2007), but in good agreement with previous measurements in humans and in the anesthetized or awake rat brain (Gruetter *et al.* 2001; Sibson *et al.* 2001; Oz *et al.* 2004; Duarte *et al.* 2011). The value found for the pyruvate carboxylase flux under infusion of [2-$^{13}C_2$]acetate was 26% higher than the value found under [1,6-$^{13}C_2$]glucose infusion (Duarte *et al.* 2011), consistent with the slow increase of mass in the glutamate and glutamine pools when infusing sodium acetate.

Overall, the values found for the different fluxes are in very good agreement with the values found in previous [1,6-$^{13}C_2$]glucose infusion studies (Duarte *et al.* 2011) and with the values recently found using [1-^{11}C]acetate infusion in positron emission studies in rats (Lanz *et al.* 2012) (Table 2). Compared to glucose infusion studies, fewer labeling curves (GluC4, GlnC4, GluC3, and GlnC3) were needed to achieve similar or better precision on the glial metabolic fluxes or the neurotransmission rate.

Effect of glutamate and glutamine pool distribution

To determine the influence of differential distribution of glutamine (predominantly glial) and glutamate (predominantly neuronal), we analyzed the sensitivity of the glutamate and glutamine uptake curve to these assumptions. Replacing the glial glutamine and neuronal glutamine pools by a single kinetic compartment had a negligible effect on the dynamics of the turnover curves and, consequently, on the derived metabolic fluxes (data not shown). This can be understood by the fact that glutamine participates in only two biochemical reactions, namely glutamine synthesis in the glia (V_{GS}) and the phosphate-activated glutaminase (PAG) in neurons, in contrast to glutamate. The large glial glutamine pool is the only precursor of the neuronal glutamine pool, which is only a small fraction of total glutamine (Storm-Mathisen *et al.* 1992). The labeling dynamics of neuronal glutamine is therefore much faster than glial glutamine and the neuronal pool is basically following the enrichment of its precursor, which results in very similar FEs in both glutamine pools.

It is well established that tissue glutamate in brain is unequally distributed between the neuronal and glial compartments (Storm-Mathisen *et al.* 1992). In early studies, the presence of two distinct glutamate pools was proposed from ^{14}C labeling studies in mice (van den Berg and Garfinkel 1971), reporting a small glutamate pool with a concentration of 1.3 μmol/g and a large neuronal pool of 7 μmol/g. Using immunochemical methods (Ottersen *et al.* 1992; Storm-Mathisen *et al.* 1992), it was found that most of glutamate is in the neuronal compartment, while glutamine is mostly located in astrocytes. A glutamate to glutamine ratio of 0.2 in astrocytes was reported, which is in good agreement with the values found in our study, if all glutamine is assumed to be in the glial compartment (0.6 μmol/g for Glu^g with 3.4 μmol/g of Gln).

The dilution from pyruvate metabolism at the level of glial acetyl-CoA, represented by K_{dil} [Fig. 1a and Appendix, eqns (8) and (9)], could be theoretically extracted from the steady-state enrichment of the glutamine labeling positions. However, when fitting the model and including K_{dil} as free parameter, the value found for K_{dil} was subject to high uncertainty and was strongly correlated with the glial TCA cycle flux and transmitochondrial flux (data not shown). In the case of acetate infusion, K_{dil} is expected to be at least as high as the value found with glucose infusion [0.76 in (Duarte *et al.* 2011)], because of higher amount of available plasma acetate. A 10% increase in K_{dil} resulted in a decrease of 11% and 35% in V_g and V_x^g, respectively, while all the other fluxes and the determined glial glutamate concentration were marginally affected (< 4%). The conclusions of this study are therefore not affected by the assumption on glial acetyl-CoA dilution.

The transport of acetate across the blood-brain barrier (BBB) may be rate-limiting, however, the acetate infusion of our experiments resulted in a step-wise increase in plasma acetate concentration to 9 mM, where transport across the BBB was shown not to be rate-limiting for metabolism (Deelchand *et al.* 2009b). Note that in this study, we used the NMR-measured brain acetate ^{13}C enrichment as direct input to the metabolic system, which minimizes the impact of acetate transport on the metabolic flux determination.

The metabolic model used for [2-^{13}C]acetate labeling studies is based on the assumption of the purely glial uptake and metabolism of acetate (Lebon *et al.* 2002; Deelchand

Table 2 Comparison of the determined metabolic fluxes (μmol/g/min) obtained infusing ^{13}C-acetate, ^{13}C-glucose (Duarte *et al.* 2011) or ^{11}C-acetate (Lanz *et al.* 2012), a positron emitting radiotracer

Brain metabolic fluxes (in μmol/g/min) obtained with different labeled substrates

Substrate	V_g	V_x^g	V_{PC}	V_{gt}^g	V_{NT}	V_{tca}^n	V_x^n	V_{gt}^n
[2-^{13}C]acetate	0.27 ± 0.02	0.17 ± 0.02	0.09 ± 0.01	0.17 ± 0.01	0.15 ± 0.01	0.37 ± 0.06	0.46 ± 0.05	0.21 ± 0.02
[1,6-$^{13}C_2$]glucose[a]	0.23 ± 0.02	0.17 ± 0.06	0.07 ± 0.01	0.15 ± 0.02	0.12 ± 0.01	0.44 ± 0.01	0.76 ± 0.07	0.28 ± 0.01
[1-^{11}C]acetate[b]	–	–	–	0.14 ± 0.04	0.17 ± 0.10	–	–	–

[a](Duarte *et al.* 2011).
[b](Lanz *et al.* 2012).

et al. 2009b; Patel *et al.* 2010). At low plasma level, acetate is known to be transported primarily into glial cells (Waniewski and Martin 1998). At higher plasma acetate concentrations as used for *in vivo* studies, the passive diffusion of acetate through the cell membrane and its metabolism through acetate thiokinase both in the glial cells and the neurons could be possible. However, several previous ^{13}C-acetate infusion studies showed evidences for the predominantly glial uptake and metabolism, even at higher plasma acetate levels (Badar-Goffer *et al.* 1990; Hassel *et al.* 1995). At the end of our labeling experiment, the FE of glutamate C4 reached 15%, while glutamine C4 FE was about 35%. Since about 90% of glutamate is located in the neuronal compartment, the glutamate C4 enrichment curve represents essentially the neuronal glutamate C4 pool. The large difference between the FE of neuronal glutamate and its precursor in the glutamate/glutamine cycle indicates a strong dilution of neuronal glutamate through transmitochondrial exchange with the neuronal TCA cycle and supports the fact that neurons metabolize predominantly other substrates than acetate, even at relatively high plasma acetate concentrations. Moreover, based on previously measured metabolic fluxes (Duarte *et al.* 2011) and the FE of Glu C4 and Gln C4 obtained in the near steady-state conditions at the end of the experiment, the FE of the neuronal acetyl-CoA was estimated to be lower than 5%, which confirms that in our experimental conditions, acetate is not or marginally used as substrate by neurons.

When infusing [2-^{13}C]sodium acetate, we observed an increase of about 20% over 3 hours both in the total glutamate and total glutamine concentrations, consistent with previous *in vivo* studies (Chowdhury *et al.* 2007; Deelchand *et al.* 2009b; Patel *et al.* 2010), which could be related to an osmotic effect induced by the infusion of sodium acetate, as previously discussed (Deelchand *et al.* 2009b; Patel *et al.* 2010). The metabolic model was adapted to take into account the increase in pool size by assuming that new carbon chains are synthesized via pyruvate carboxylase. Note that the measured accumulation of glutamate and glutamine over 150 min, although statistically significant, was modest (24% for glutamate and 16% for glutamine) and did not affect significantly the dynamics of brain metabolism, since the measured fluxes are in good agreement with the metabolic fluxes obtained with ^{13}C labeled glucose infusion, where no significant change in amino acid concentration was measured (Table 2). Brain metabolic fluxes determined with two-compartment modeling, and in particular the transmitochondrial fluxes V_x^g and V_x^n, are thus largely independent on the substrate used.

To determine the consequence of the mass increase in glutamate and glutamine on the modeling results, we adjusted the metabolic model to the measured curve, assuming constant glutamate and glutamine total concentrations, equal to their respective average value over the entire infusion time. With this assumption, the neuronal TCA cycle flux was 20% smaller, while V_x^g and V_{PC} were, respectively, increased by

40% and decreased by 50%. The changes in the remaining metabolic fluxes were within 10%. As a consequence, the increase in glutamate and glutamine pool sizes appears to be an important aspect to take into account in the metabolic model to avoid biased determination of the metabolic fluxes.

Recent studies indicated that astrocytic energy metabolism is more intense as previously believed, suggesting a major involvement of glial cells in functional activities. ^{14}C-acetate autoradiography experiments showed that the TCA cycle activity increases in astrocytes during acoustic or visual stimulations (Dienel and Hertz 2001; Cruz *et al.* 2005), indicating that astrocytic respiration can be up-regulated by signaling mechanisms. The glial-specific pyruvate carboxylation increases during some but not all stimulations, while pathological conditions might also activate glial oxidative demand (Hertz *et al.* 2007). It remains also unclear if glial glutamate oxidation changes during activation *in vivo*. There are therefore many motivations to develop quantitative *in vivo* metabolic studies such as the presented ^{13}C-acetate MRS approach, to better understand the particular role of astrocytic metabolism in brain function.

Conclusion

We conclude that when using [2-^{13}C]acetate, two-compartment modeling of the C4 and C3 labeling curves of glutamate and glutamine obtained with ^{1}H-[^{13}C] MRS enables the measurement of mitochondrial metabolism both in the glial and neuronal compartment *in vivo*. In particular, the predominant glial uptake of acetate allows a precise determination of the glial metabolic fluxes and the apparent glutamatergic neurotransmission rate. In this study, the transmitochondrial exchange rates between glutamate and 2-oxoglutarate were determined separately for the glial and neuronal compartments, based on the analysis of the C3 uptake curves of glutamate and glutamine measurable at high magnetic field. Moreover, we provided the first *in vivo* estimation of the glial glutamate pool size in the rat brain tissue. ^{13}C-acetate infusion studies are therefore an attractive alternative to the more widely used ^{13}C-glucose infusions for studying pathological or physiological alterations of glial oxidative metabolism.

References

Amaral A. I., Teixeira A. P., Haakonsen B. I., Sonnewald U. and Alves P. M. (2011) A comprehensive metabolic profile of cultured astrocytes using isotopic transient metabolic flux analysis and 13C-labeled glucose. *Front. Neuroenergetics* **3**, 5.

Araque A., Parpura V., Sanzgiri R. P. and Haydon P. G. (1999) Tripartite synapses: glia, the unacknowledged partner. *Trends Neurosci.* **22**, 208–215.

Arriza J. L., Fairman W. A., Wadiche J. I., Murdoch G. H., Kavanaugh M. P. and Amara S. G. (1994) Functional comparisons of three glutamate transporter subtypes cloned from human motor cortex. *J. Neurosci.* **14**, 5559–5569.

Badar-Goffer R. S., Bachelard H. S. and Morris P. G. (1990) Cerebral metabolism of acetate and glucose studied by 13C-n.m.r. spectroscopy. A technique for investigating metabolic compartmentation in the brain. *Biochem. J.* **266**, 133–139.

van den Berg C. J. and Garfinkel D. (1971) A stimulation study of brain compartments. Metabolism of glutamate and related substances in mouse brain. *Biochem. J.* **123**, 211–218.

Cerdan S., Kunnecke B. and Seelig J. (1990) Cerebral metabolism of $[1,2-^{13}C_2]$acetate as detected by in vivo and in vitro ^{13}C NMR. *J. Biol. Chem.* **265**, 12916–12926.

Choi I. Y., Lei H. and Gruetter R. (2002) Effect of deep pentobarbital anesthesia on neurotransmitter metabolism in vivo: on the correlation of total glucose consumption with glutamatergic action. *J. Cereb. Blood Flow Metab.* **22**, 1343–1351.

Chowdhury G. M., Gupta M., Gibson K. M., Patel A. B. and Behar K. L. (2007) Altered cerebral glucose and acetate metabolism in succinic semialdehyde dehydrogenase-deficient mice: evidence for glial dysfunction and reduced glutamate/glutamine cycling. *J. Neurochem.* **103**, 2077–2091.

Cruz N. F., Lasater A., Zielke H. R. and Dienel G. A. (2005) Activation of astrocytes in brain of conscious rats during acoustic stimulation: acetate utilization in working brain. *J. Neurochem.* **92**, 934–947.

Danbolt N. C. (2001) Glutamate uptake. *Prog. Neurobiol.* **65**, 1–105.

Deelchand D. K., Nelson C., Shestov A. A., Ugurbil K. and Henry P. G. (2009a) Simultaneous measurement of neuronal and glial metabolism in rat brain in vivo using co-infusion of $[1,6-^{13}C_2]$ glucose and $[1,2-^{13}C_2]$acetate. *J. Magn. Reson.* **196**, 157–163.

Deelchand D. K., Shestov A. A., Koski D. M., Ugurbil K. and Henry P. G. (2009b) Acetate transport and utilization in the rat brain. *J. Neurochem.* **109**(Suppl 1), 46–54.

Dienel G. A. (2011) Brain lactate metabolism: the discoveries and the controversies. *J. Cereb. Blood Flow Metab.* **32**, 1107–1138.

Dienel G. A. and Hertz L. (2001) Glucose and lactate metabolism during brain activation. *J. Neurosci. Res.* **66**, 824–838.

Duarte J. M. N., Lanz B. and Gruetter R. (2011) Compartmentalized cerebral metabolism of [1,6-13C]glucose determined by in vivo 13C NMR spectroscopy at 14.1 T. *Front. Neuroenergetics* **3**, 3.

van Eijsden P., Behar K. L., Mason G. F., Braun K. P. and de Graaf R. A. (2010) In vivo neurochemical profiling of rat brain by ^{1}H-$[^{13}C]$ NMR spectroscopy: cerebral energetics and glutamatergic/GABAergic neurotransmission. *J. Neurochem.* **112**, 24–33.

de Graaf R. A., Brown P. B., Mason G. F., Rothman D. L. and Behar K. L. (2003a) Detection of $[1,6-^{13}C_2]$-glucose metabolism in rat brain by in vivo ^{1}H-$[^{13}C]$-NMR spectroscopy. *Magn. Reson. Med.* **49**, 37–46.

de Graaf R. A., Mason G. F., Patel A. B., Behar K. L. and Rothman D. L. (2003b) In vivo ^{1}H-$[^{13}C]$-NMR spectroscopy of cerebral metabolism. *NMR Biomed.* **16**, 339–357.

de Graaf R. A., Mason G. F., Patel A. B., Rothman D. L. and Behar K. L. (2004) Regional glucose metabolism and glutamatergic neurotransmission in rat brain in vivo. *Proc. Natl Acad. Sci. USA* **101**, 12700–12705.

Gruetter R. and Tkac I. (2000) Field mapping without reference scan using asymmetric echo-planar techniques. *Magn. Reson. Med.* **43**, 319–323.

Gruetter R., Seaquist E. R. and Ugurbil K. (2001) A mathematical model of compartmentalized neurotransmitter metabolism in the human brain. *Am. J. Physiol. Endocrinol. Metab.* **281**, E100–E112.

Gulanski B. I., De Feyter H. M., Page K. A., de Aguiar R. B., Mason G. F., Rothman D. L. and Sherwin R. S. (2013) Increased Brain Transport and Metabolism of Acetate in Hypoglycemia Unawareness. *J. Clin. Endocrinol. Metab.* **98**, 3811–3820.

Hassel B., Sonnewald U. and Fonnum F. (1995) Glial-neuronal interactions as studied by cerebral metabolism of [2-13C]acetate and [1-13C]glucose: an ex vivo 13C NMR spectroscopic study. *J. Neurochem.* **64**, 2773–2782.

Henry P. G., Lebon V., Vaufrey F., Brouillet E., Hantraye P. and Bloch G. (2002) Decreased TCA cycle rate in the rat brain after acute 3-NP treatment measured by in vivo ^{1}H-$[^{13}C]$ NMR spectroscopy. *J. Neurochem.* **82**, 857–866.

Henry P. G., Adriany G., Deelchand D., Gruetter R., Marjanska M., Oz G., Seaquist E. R., Shestov A. and Ugurbil K. (2006) In vivo ^{13}C NMR spectroscopy and metabolic modeling in the brain: a practical perspective. *Magn. Reson. Imaging* **24**, 527–539.

Hertz L. (2011) Astrocytic energy metabolism and glutamate formation–relevance for 13C-NMR spectroscopy and importance of cytosolic/mitochondrial trafficking. *Magn. Reson. Imaging* **29**, 1319–1329.

Hertz L., Peng L. and Dienel G. A. (2007) Energy metabolism in astrocytes: high rate of oxidative metabolism and spatiotemporal dependence on glycolysis/glycogenolysis. *J. Cereb. Blood Flow Metab.* **27**, 219–249.

Hyder F., Chase J. R., Behar K. L., Mason G. F., Siddeek M., Rothman D. L. and Shulman R. G. (1996) Increased tricarboxylic acid cycle flux in rat brain during forepaw stimulation detected with ^{1}H$[^{13}C]$ NMR. *Proc. Natl Acad. Sci. USA* **93**, 7612–7617.

Jiang L., Gulanski B. I., De Feyter H. M. *et al.* (2013) Increased brain uptake and oxidation of acetate in heavy drinkers. *J. Clin. Invest.* **123**, 1605–1614.

Lanz B., Uffmann K., Wyss M. T., Weber B., Buck A. and Gruetter R. (2012) A two-compartment mathematical model of neuroglial metabolism using [1-(11)C] acetate. *J. Cereb. Blood Flow Metab.* **32**, 548–559.

Lebon V., Petersen K. F., Cline G. W., Shen J., Mason G. F., Dufour S., Behar K. L., Shulman G. I. and Rothman D. L. (2002) Astroglial contribution to brain energy metabolism in humans revealed by ^{13}C nuclear magnetic resonance spectroscopy: elucidation of the dominant pathway for neurotransmitter glutamate repletion and measurement of astrocytic oxidative metabolism. *J. Neurosci.* **22**, 1523–1531.

Mason G. F. and Rothman D. L. (2004) Basic principles of metabolic modeling of NMR ^{13}C isotopic turnover to determine rates of brain metabolism in vivo. *Metab. Eng.* **6**, 75–84.

Mason G. F., Rothman D. L., Behar K. L. and Shulman R. G. (1992) NMR determination of the TCA cycle rate and alpha-ketoglutarate/glutamate exchange rate in rat brain. *J. Cereb. Blood Flow Metab.* **12**, 434–447.

Mason G. F., Gruetter R., Rothman D. L., Behar K. L., Shulman R. G. and Novotny E. J. (1995) Simultaneous determination of the rates of the TCA cycle, glucose utilization, alpha-ketoglutarate/glutamate exchange, and glutamine synthesis in human brain by NMR. *J. Cereb. Blood Flow Metab.* **15**, 12–25.

Mason G. F., Petersen K. F., de Graaf R. A., Shulman G. I. and Rothman D. L. (2007) Measurements of the anaplerotic rate in the human cerebral cortex using 13C magnetic resonance spectroscopy and [1-13C] and [2-13C] glucose. *J. Neurochem.* **100**, 73–86.

McKenna M. C. (2012) Substrate competition studies demonstrate oxidative metabolism of glucose, glutamate, glutamine, lactate and 3-hydroxybutyrate in cortical astrocytes from rat brain. *Neurochem. Res.* **37**, 2613–2626.

Mishkovsky M., Comment A. and Gruetter R. (2012) In vivo detection of brain Krebs cycle intermediate by hyperpolarized magnetic resonance. *J. Cereb. Blood Flow Metab.* **32**, 2108–2113.

Ottersen O. P., Zhang N. and Walberg F. (1992) Metabolic compartmentation of glutamate and glutamine: morphological evidence obtained by quantitative immunocytochemistry in rat cerebellum. *Neuroscience* **46**, 519–534.

Oz G., Berkich D. A., Henry P. G., Xu Y., LaNoue K., Hutson S. M. and Gruetter R. (2004) Neuroglial metabolism in the awake rat brain: CO$_2$ fixation increases with brain activity. *J. Neurosci.* **24**, 11273–11279.

Patel A. B., de Graaf R. A., Mason G. F., Rothman D. L., Shulman R. G. and Behar K. L. (2005) The contribution of GABA to glutamate/glutamine cycling and energy metabolism in the rat cortex in vivo. *Proc. Natl Acad. Sci. USA* **102**, 5588–5593.

Patel A. B., de Graaf R. A., Rothman D. L., Behar K. L. and Mason G. F. (2010) Evaluation of cerebral acetate transport and metabolic rates in the rat brain in vivo using ^{1}H-[^{13}C]-NMR. *J. Cereb. Blood Flow Metab.* **30**, 1200–1213.

Rothstein J. D., Dykes-Hoberg M., Pardo C. A. *et al.* (1996) Knockout of glutamate transporters reveals a major role for astroglial transport in excitotoxicity and clearance of glutamate. *Neuron* **16**, 675–686.

Shank R. P., Leo G. C. and Zielke H. R. (1993) Cerebral metabolic compartmentation as revealed by nuclear magnetic resonance analysis of D-[1-13C]glucose metabolism. *J. Neurochem.* **61**, 315–323.

Shestov A. A., Valette J., Ugurbil K. and Henry P. G. (2007) On the reliability of ^{13}C metabolic modeling with two-compartment neuronal-glial models. *J. Neurosci. Res.* **85**, 3294–3303.

Shestov A. A., Valette J., Deelchand D. K., Ugurbil K. and Henry P. G. (2012) Metabolic modeling of dynamic brain ^{13}C NMR multiplet data: concepts and simulations with a two-compartment neuronal-glial model. *Neurochem. Res.* **37**, 2388–2401.

Sibson N. R., Dhankhar A., Mason G. F., Rothman D. L., Behar K. L. and Shulman R. G. (1998) Stoichiometric coupling of brain glucose metabolism and glutamatergic neuronal activity. *Proc. Natl Acad. Sci. USA* **95**, 316–321.

Sibson N. R., Mason G. F., Shen J., Cline G. W., Herskovits A. Z., Wall J. E., Behar K. L., Rothman D. L. and Shulman R. G. (2001) In vivo ^{13}C NMR measurement of neurotransmitter glutamate cycling, anaplerosis and TCA cycle flux in rat brain during. *J. Neurochem.* **76**, 975–989.

Sokoloff L. (1977) Relation between physiological function and energy metabolism in the central nervous system. *J. Neurochem.* **29**, 13–26.

Storm-Mathisen J., Danbolt N. C., Rothe F., Torp R., Zhang N., Aas J. E., Kanner B. I., Langmoen I. and Ottersen O. P. (1992) Ultrastructural immunocytochemical observations on the localization, metabolism and transport of glutamate in normal and ischemic brain tissue. *Prog. Brain Res.* **94**, 225–241.

Uffmann K. and Gruetter R. (2007) Mathematical modeling of ^{13}C label incorporation of the TCA cycle: the concept of composite precursor function. *J. Neurosci. Res.* **85**, 3304–3317.

Waniewski R. A. and Martin D. L. (1998) Preferential utilization of acetate by astrocytes is attributable to transport. *J. Neurosci.* **18**, 5225–5233.

Wyss M. T., Weber B., Treyer V., Heer S., Pellerin L., Magistretti P. J. and Buck A. (2009) Stimulation-induced increases of astrocytic oxidative metabolism in rats and humans investigated with 1-^{11}C-acetate. *J. Cereb. Blood Flow Metab.* **29**, 44–56.

Xin L., Mlynarik V., Lanz B., Frenkel H. and Gruetter R. (2010) ^{1}H-[^{13}C] NMR spectroscopy of the rat brain during infusion of [2-^{13}C] acetate at 14.1 T. *Magn. Reson. Med.* **64**, 334–340.

Yudkoff M., Nissim I., Daikhin Y., Lin Z. P., Nelson D., Pleasure D. and Erecinska M. (1993) Brain glutamate metabolism: neuronal-astroglial relationships. *Dev. Neurosci.* **15**, 343–350.

Appendix

The mathematical model of compartmentalized cerebral metabolism was adapted from (Gruetter *et al.* 2001), where the reader can find an exhaustive description of the model.

The metabolic pools and fluxes of the considered model are represented in Fig. 1. Metabolic steady-state was assumed for the metabolic fluxes (constant) and the metabolic pools except glutamine and the major neuronal glutamate pools, which total concentration was slightly increasing over time, as measured by ^{1}H MRS. The *in vivo* measured mean glutamate and glutamine concentrations were 11.5 and 3.4 μmol/g, respectively. As determined in this study, 0.6 μmol/g of glutamate was contained in the glial compartment, while all the glutamine was assumed to be glial.

The non-steady-state conditions for glutamine and neuronal glutamate was modeled using the following mass-balance equations. dGlu/dt and dGln/dt are the slopes of the increase in total glutamate and total glutamine concentrations, respectively, as measured by ^{1}H MRS:

$$V_{GS} - V_{efflux} - V_{Glu} = \frac{dGln}{dt}$$

$$with\ V_{GS} = V_{NT} + V_{PC} \tag{6}$$

$$V_{Glu} - V_{NT} = \frac{dGlu}{dt} \tag{7}$$

The mass balance relations shown in eqns (6) and (7) were further used as constraints in the metabolic model, i.e. V_{NT} and V_{PC} are adjusted in the fitting of the ^{13}C turnover curves, while V_{efflux}, V_{Glu}, and V_{GS} are then determined from eqns (6) and (7).

Transport of acetate across the blood–brain barrier was not modeled, as brain acetate FE was directly measured with ^{1}H-[^{13}C] MRS and used as input function for the model.

Glial compartment

Pyruvate and acetate compete for the generation of acetyl-CoA:

The position 2 of glial acetyl-CoA is labeled as follows:

$$\frac{dAcCoA_2^g}{dt} = V_{Ace}\frac{Ace_2(t)}{Ace} - \left(V_{Ace} + V_{dil}^g\right)\frac{AcCoA_2^g(t)}{AcCoA} \tag{8}$$

where V_{Ace} is the net metabolic flux of acetate to acetyl-CoA and V_{dil}^g is the dilution flux from the metabolism of unlabeled pyruvate in the glial compartment. Working with the small pool approximation for glial acetyl-CoA (Uffmann and Gruetter 2007) ($\frac{dAcCo_2^g}{dt} \cong 0$ very early compared with the large glutamate pool), we obtain the following relationship between the fractional enrichment of $AcCoA_2^g$ and plasma Ace_2:

$$\frac{AcCoA_2^g(t)}{AcCoA} = \frac{V_{Ace}}{\left(V_{Ace} + V_{dil}^g\right)}\frac{Ace_2(t)}{Ace} \equiv K_{dil}\frac{Ace_2(t)}{Ace} \tag{9}$$

K_{dil} represents the affinity of glial cells to acetate as metabolic fuel. It was fixed to the value found with ^{13}C NMR in a recent study (Duarte *et al.* 2011), $K_{dil} = 0.76$.

Further metabolism of acetate in the glial compartment is characterized by the glial TCA cycle flux V_g, the transmitochondrial exchange between 2-oxoglutarate and glutamate V_x^g and pyruvate carboxylase V_{PC}.

In the glial TCA cycle, the labeling of 2-oxoglutarate is given by the following equations:

$$\frac{dOG_4^g}{dt} = K_{dil}(V_g + V_{PC})\frac{Ace_2(t)}{Ace} + V_x^g \frac{Glu_4^g(t)}{Glu^g}$$
$$- (V_x^g + V_{PC} + V_g)\frac{OG_4^g(t)}{OG^g} \qquad (10)$$

$$\frac{dOG_3^g}{dt} = \frac{V_g}{2}\frac{OG_4^g(t)}{OG^g} + V_x^g \frac{Glu_3^g(t)}{Glu^g} - \left(V_x^g + V_{PC} + \frac{V_g}{2}\right)\frac{OG_3^g(t)}{OG^g} \qquad (11)$$

The factor ½ appearing in eqn (11) is related to the fact that in each TCA cycle turn, half of the labeling from OG_4^g goes to OG_3^g and half of it goes to OG_2^g, because of the symmetry of the succinate molecule (Uffmann and Gruetter 2007). Similarly, half of the labeling from OG_3^g goes to OG_2^g and half of it comes back to OG_3^g.

The labeling of glial glutamate is given by the following equations:

$$\frac{dGlu_4^g}{dt} = (V_x^g + V_{PC})\frac{OG_4^g(t)}{OG^g}$$
$$+ V_{NT}\frac{Glu_4^n(t)}{Glu^n(t)} - (V_x^g + V_{GS})\frac{Glu_4^g(t)}{Glu^g} \qquad (12)$$

$$\frac{dGlu_3^g}{dt} = (V_x^g + V_{PC})\frac{OG_3^g(t)}{OG^g} + V_{NT}\frac{Glu_3^n(t)}{Glu^n(t)}$$
$$- (V_x^g + V_{GS})\frac{Glu_3^g(t)}{Glu^g} \qquad (13)$$

Removing the (non-measurable) TCA cycle intermediates from the model

We made use of a simplification of the metabolic model by removing the TCA cycle intermediates from the labeling equations, as suggested in previous studies (Uffmann and Gruetter 2007; Duarte *et al.* 2011). This results in mathematical expressions which do not contain non-measurable metabolic pools, while the effect of the simplification on the determined metabolic fluxes is marginal.

By injecting in eqn (12) the expression of $\frac{OG_4^g}{OG^g}$ isolated in eqn (10), we obtain the following:

$$\frac{dGlu_4^g}{dt} = (V_x^g + V_{PC})\left[\frac{K_{dil}(V_g + V_{PC})}{(V_x^g + V_{PC} + V_g)}\frac{Ace_2(t)}{Ace}\right.$$
$$\left. + \frac{V_x^g}{(V_x^g + V_{PC} + V_g)}\frac{Glu_4^g(t)}{Glu^g} - \frac{1}{(V_x^g + V_{PC} + V_g)}\frac{dOG_4^g}{dt}\right]$$
$$+ V_{NT}\frac{Glu_4^n(t)}{Glu^n(t)} - (V_x^g + V_{GS})\frac{Glu_4^g(t)}{Glu^g} \qquad (14)$$

$$\frac{dGlu_4^g}{dt} + \frac{(V_x^g + V_{PC})}{(V_x^g + V_{PC} + V_g)}\frac{dOG_4^g}{dt}$$
$$= \frac{K_{dil}(V_g + V_{PC})(V_x^g + V_{PC})}{(V_x^g + V_{PC} + V_g)}\frac{Ace_2(t)}{Ace} \qquad (15)$$
$$+ \frac{V_x^g(V_x^g + V_{PC})}{(V_x^g + V_{PC} + V_g)}\frac{Glu_4^g(t)}{Glu^g} + V_{NT}\frac{Glu_4^n(t)}{Glu^n(t)}$$
$$- (V_x^g + V_{GS})\frac{Glu_4^g(t)}{Glu^g}$$

In the small pool approximation, we assume that the increase in glutamate enriched carbons is much larger than the increase in 2-oxoglutarate ^{13}C concentration, i.e. $\frac{dOG_4^g}{dt} \ll \frac{dGlu_4^g}{dt}$. This approximation is as much better that the time after the start of the infusion gets larger, since the small pool reaches its labeling steady-state faster than the larger pool. The small pool approximation leads to the following expression for the labeling of glial glutamate C4, in which the TCA cycle intermediate pools vanished:

$$\frac{dGlu_4^g}{dt} = \frac{K_{dil}(V_g + V_{PC})(V_x^g + V_{PC})}{(V_x^g + V_{PC} + V_g)}\frac{Ace_2(t)}{Ace}$$
$$+ \frac{V_x^g(V_x^g + V_{PC})}{(V_x^g + V_{PC} + V_g)}\frac{Glu_4^g(t)}{Glu^g} + V_{NT}\frac{Glu_4^n(t)}{Glu^n(t)}$$
$$- (V_x^g + V_{GS})\frac{Glu_4^g(t)}{Glu^g} \qquad (16)$$

Using the same strategy for glial glutamate C3, we obtain the following expression:

$$\frac{dGlu_3^g}{dt} = \frac{K_{dil}(V_g + V_{PC})(V_x^g + V_{PC})}{V_x^g + V_{PC} + V_g}\frac{V_g}{2V_x^g + 2V_{PC} + V_g}$$
$$\times \frac{Ace_2(t)}{Ace} + \frac{V_g(V_x^g + V_{PC})}{V_x^g + V_{PC} + V_g}\frac{V_x^g}{2V_x^g + 2V_{PC} + V_g}$$
$$\times \frac{Glu_4^g(t)}{Glu^g} + V_x^g \frac{V_x^g + V_{PC}}{\left(V_x^g + V_{PC} + \frac{V_g}{2}\right)}\frac{Glu_3^g(t)}{Glu^g}$$
$$+ V_{NT}\frac{Glu_3^n(t)}{Glu^n(t)} - (V_x^g + V_{GS})\frac{Glu_3^g(t)}{Glu^g} \qquad (17)$$

Neuronal compartment

Acetate is considered not to be metabolized in the neuronal compartment. Pyruvate carboxylase is also absent in the neurons. ^{13}C is therefore entering the neuronal TCA cycle through its interaction with the neuronal glutamate pool. In the neuronal compartment, the labeling of the TCA intermediates and the neuronal glutamate pools is given by:

$$\frac{dOG_4^n}{dt} = V_x^n \frac{Glu_4^n(t)}{Glu^n(t)} - (V_x^n + V_{tca}^n) \frac{OG_4^n(t)}{OG^n} \quad (18)$$

$$\frac{dOG_3^n}{dt} = \frac{V_{tca}^n}{2} \frac{OG_4^n(t)}{OG^n} + V_x^g \frac{Glu_3^n(t)}{Glu^n(t)} - \left(V_x^n + \frac{V_{tca}^n}{2}\right) \frac{OG_3^n(t)}{OG^n} \quad (19)$$

$$\frac{dGlu_4^n}{dt} = V_x^n \frac{OG_4^n(t)}{OG^n} + V_{Glu} \frac{Gln_4(t)}{Gln(t)} - (V_x^n + V_{NT}) \frac{Glu_4^n(t)}{Glu^n(t)} \quad (20)$$

$$\frac{dGlu_3^n}{dt} = V_x^n \frac{OG_3^n(t)}{OG^n} + V_{Glu} \frac{Gln_3(t)}{Gln(t)} - (V_x^n + V_{NT}) \frac{Glu_3^n(t)}{Glu^n(t)} \quad (21)$$

Using the same approach as for the glial glutamate pools, the TCA cycle intermediates can be eliminated from the differential equations describing the labeling of the neuronal glutamate pools:

$$\frac{dGlu_4^n}{dt} = V_x^n \frac{V_x^n}{(V_x^n + V_{tca}^n)} \frac{Glu_4^n(t)}{Glu^n(t)} + V_{Glu} \frac{Gln_4(t)}{Gln(t)} - (V_x^n + V_{NT}) \frac{Glu_4^n(t)}{Glu^n(t)} \quad (22)$$

$$\frac{dGlu_3^n}{dt} = \frac{V_{tca}^n V_x^n}{V_x^n + V_{tca}^n} \frac{V_x^n}{2V_x^n + V_{tca}^n} \frac{Glu_4^n(t)}{Glu^n(t)} + V_x^n \frac{V_x^n}{\left(V_x^n + \frac{V_{tca}^n}{2}\right)} \frac{Glu_3^n(t)}{Glu^n(t)} + V_{Glu} \frac{Gln_3(t)}{Gln(t)} - (V_x^n + V_{NT}) \frac{Glu_3^n(t)}{Glu^n(t)} \quad (23)$$

Glutamate–glutamine cycle

The glutamate-glutamine cycle comprises the glutamine synthesis in the glial compartment, the transfer of glutamine to neurons where it is converted back to glutamate and stored in the large neuronal glutamate pool and finally the glutamatergic neurotransmission where glutamate is released from the neurons and taken up by the glial compartment. The labeling equations of glutamine, modeled as a single large glial pool, are as follows:

$$\frac{dGln_4}{dt} = V_{GS} \frac{Glu_4^g(t)}{Glu^g} - (V_{efflux} + V_{Glu}) \frac{Gln_4(t)}{Gln(t)} \quad (24)$$

$$\frac{dGln_3}{dt} = V_{GS} \frac{Glu_3^g(t)}{Glu^g} - (V_{efflux} + V_{Glu}) \frac{Gln_3(t)}{Gln(t)} \quad (25)$$

where V_{efflux} accounts for the label loss through glutamine dilution. V_{GS}, V_{efflux}, and V_{Glu} are modeled to take into account the non-steady-state concentrations of glutamate and glutamine measured under sodium acetate infusion. They are coupled with V_{NT} by the eqn (6) and (7) where the increase of glutamate and glutamine, measured by ^{1}H MRS is used in the mass balance equations. Therefore, when fitting the ^{13}C enrichment curves, only one degree of freedom is adjusted for the glutamate-glutamine cycle, namely V_{NT}, while V_{GS}, V_{efflux} and V_{Glu} are determined from the mass balance equations.